# A lamb wave-based icing sensor for aircraft ice detection

Martin Pohl[1]

[1] *German Aerospace Center (DLR), Braunschweig, Germany*

martin.pohl@dlr.de

*Abstract*— **Ice accretion is a still an issue in modern aviation since icing meteorological conditions can occur within the flight. If an aircraft hits such conditions, the amount of ice accreting on the airplane can have substantial influence on weight and loss of aerodynamic performance, which may be even fatal. Especially supercooled large droplet (SLD) icing is critical due to a high accretion rate and the risk of runback ice on the airfoil. Until now, aircraft are losing control due to severe icing, which is not recognized fast enough by the pilots to react either by activating ice protection or by leaving the icing conditions instantly.**

**To ensure fast reactions, a sensor would be helpful to detect ice accretion on susceptible surfaces, such as leading edges of wings and empennage of aircraft. This would not only enable fast detection of severe icing, but also allow to use thermal anti-icing systems only then when it is really necessary. Due to the high power consumption of such systems, this may lead to fuel saving.**

**Within the EU project SENS4ICE, such a sensor has been developed and tested by the German Aerospace Center (DLR). It uses travelling ultrasonic lamb waves, which are sent though the structure, which is prone to ice accretion. The presence of ice alters the waveguide behaviour of the underlying structure, which can be detected. In the project, a sensor design is developed, prototypes are built and finally tested in an icing wind tunnel experiment. This paper will provide an overview about the measurement principle, the sensor design and present some wind tunnel results.**

**It could be shown, that ice accretion is detectable with very short delay time when happening on a clean airfoil.**

Keywords— ***Lamb wave, Piezoeffect, ultrasonic wave, ice sensor, aircraft icing, SENS4ICE***

## I. INTRODUCTION

Ice accretion happens, when atmospheric water freezes on structures. If the ice accretion is too heavy, it can lead to a functional degradation or even a catastrophic failure of the structure. This is especially the case in aviation, where airplanes regularly encounter freezing temperatures in the air as well as atmospheric water in the form of precipitation, snow or condensation. It is easy to understand, that ice accretion on an aircraft in flight has to be prevented by any means, since the ice heavily degrades the aerodynamic performance by reducing lift and increasing drag, but also adds to the aircraft weight. Therefore, aircraft have de-icing and anti-icing systems to either remove ice or prevent the accretion.

Activating these systems is by now task of the pilot in command, who, in most cases, either activates the anti-icing system of large aircraft preventively when icing conditions are forecast. On the other hand, in the case of smaller aircraft, the de-icing will be activated, when ice becomes visible. This leads to disadvantages for both aircraft. Large aircraft encounter an additional fuel consumption due to the high thermal power of thermal anti-icing systems. For small aircraft, the ice accretion may be overseen and become too serious to react. Additionally, in conditions with supercooled large droplet icing (SLD), where precipitation is cooled below freezing, a severe ice accretion takes place within seconds, which can even overwhelm the anti-icing systems of large aircraft.

To first increase the efficiency of anti-icing and de-icing methods and to prevent aircraft from staying in unexpected severe icing, an icing sensor would be extremely helpful. By this, the pilot does not have to look for ice accretion and can focus on different flying tasks. Icing encounters will not be missed, which is especially helpful for small aircraft with no ice protection or less powerful ones, since they can immediately leave the icing region. Large aircraft profit from an adjustment of the anti-icing system to the real conditions in time.

Within the EU project SENS4ICE, different icing sensors are developed and tested. There, not only the “classical” CS-25 Appendix C (App C) is considered, where icing conditions with small droplets are defined for certification. In addition, the sensors also have to be tested in Appendix O (App O) conditions, where the already mentioned SLD conditions are defined.

One sensor developed at DLR will be presented in detail in the following chapters. It is based on sending ultrasonic lamb waves through a structure, which is prone to ice accretion. Since the ice layer, which builds up on the structure, changes the stiffness, damping and the mass of the structure, these changes can be obtained by analysing the wave guide behaviour of the structure. The sensor directly measures the surface, where the ice accretion happens, and provides the results instantly. Furthermore, only two small transducers have to be added at the inside of the structure, which also makes the sensor suitable for small and large aircraft or similar structures, where ice accretion has to be measured.

Within the project, the sensor electronics have been improved to fit a flight test, which is scheduled for 2023. Initial wind tunnel tests have been undertaken to investigate the wave guide change of the structure with differing ice layers. Finally, a wind tunnel test was performed at the Technical University of Braunschweig, where the sensor was mounted on a test airfoil within the test section of the tunnel. There, multiple test points with different temperatures, liquid water contents and droplet diameters have been measured.

As a result of these test points, the sensor detected the beginning of the ice accretion in all test points with minor delay after starting the icing conditions, which makes it ideal for detecting the encounter of icing conditions.

## II. Ice Sensors on Aircraft

Icing sensors have been researched and used in the past. An overview about different commercially available ice sensors is provided in [1], where a variety of products working with different principles is shown. Generally, the sensors shown in this document can be ordered into three main principles: First detection of freezing ice on moving structures, second the change in the vibration pattern of oscillating probes and third optical measures such as high contrast paint for visual or camera detection of ice.

Moving part sensors use a rotating part, which is placed outside the aircraft within the airflow. If the aircraft hits icing conditions, ice will accrete at the rotating part hindering the movement of this part. This can be detected by a higher driving force.

Vibration sensors use an oscillating pin, which is placed in the airflow outside the aircraft. If the aircraft hits icing conditions, ice will accrete on the pin, increase its mass and by this the eigenfrequency of the pin will decrease. This can be used as sensor signal. After a certain ice accretion has happened, the pin is electrically heated to shed the ice and a new accretion cycle can happen if the icing conditions are prevailing. Currently several ice probes using this principle are under production, such as the magnetostrictive vibration probes offered by Collins Aerospace [2]. They are available in different sizes for different aircraft types.

One example of optical sensors detecting the icing conditions by sensing particles is the Collins Aerospace OID [3], which uses light and cameras to detect water or ice droplets in the air indicating icing conditions. It can be mounted flush to the aircraft.

A disadvantage of all mentioned sensors consists in their mounting location either at the fuselage or at the rim of engine nacelles. Ice can only be detected there without the possibility to judge the presence of ice at leading edges of aerodynamic surfaces. Furthermore, parts sticking out of the airframe produce drag. And especially sensors detecting icing conditions have an inherent uncertainty if the icing conditions really lead to an ice accretion. Therefore a sensor would highly be appreciated, which directly detects an ice accretion on susceptible structures, such as leading edges and which does not include parts sticking out of the airframe.

## III. Sensor Principle and Design

One promising possibility to overcome the limitation of such discrete sensors is to use the structure itself as the sensor, which is prone to icing. This can be achieved by sending ultrasonic lamb waves through the structure from a transmitter to a receiver as shown in Figure 1. This principle is called Local Ice Layer Detector (LILD).

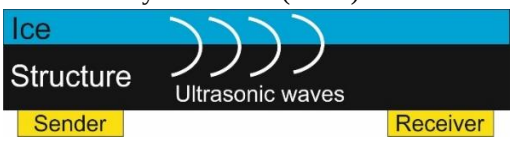


**Figure 1: LILD principle**

As the baseline structure, the skin of wing and empennage leading edge surface sheets can be used as e.g. shown in Figure 2. If ice accretion takes place on this structure, the wave guide behaviour of the structure is changed and therefore the received wave data are different.

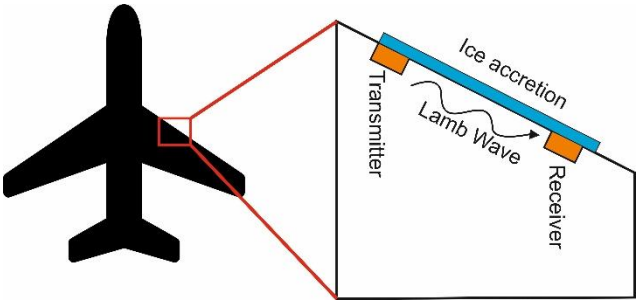


**Figure 2: Mounting location of LILD sensor at wind leading edge**

Since the main project goal of SENS4ICE is the airborne demonstration of the sensor performance with a flight test, the basic principle of the LILD sensor has to be implemented in a way that it is suited for flight tests. The following requirements have to be fulfilled:

- Generation of high frequency lamb wave signals up to 1MHz
- Measurement and filtering of received data
- Pulse identification and analysis
- Minimum power supply
- Standalone system with 28V aircraft power supply
- Data interface to communicate with other airplane systems

To transmit and receive the ultrasonic waves, piezoelectric transducers of the DuraAct P-876 type are used [4]. They incorporate a thin, 0,2 mm piezoelectric ceramic layer, which is encapsulated in resin for bending rigidity, isolation and best contacting. For a minimum sensor implementation, at least one transmitter and receiver patch are needed, which have to be connected to an electronics box. Since no high power electronics are used, this box can be kept small. It will be powered by standard 28V DC supply available on aircraft and is supposed to need less than 10W. Measurement data and information about ice accretion will be delivered to the flight information system via data bus. The basic setup is shown in Figure 3.

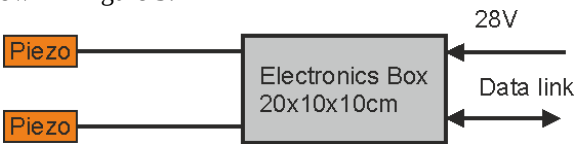


**Figure 3: Electronics input and output**

To provide signal generation, a combination of a dual core microcontroller and a FPGA is used. The FPGA allows fast signal input and output at a maximum sampling frequency of 125 MHz. It is used in the form of a Redpitaya STEMLab 125/14 board, where the FPGA functionalities are accessible via API [5].

To use this in the wind tunnel and flight test, a surrounding circuit board has been designed and built, which

incorporates a DC/DC power supply, input filters and amplifiers as well as the output amplifier and a four channel multiplexer for input and output each. Therefore four individual wave paths can be measured. A photo of the prototype board can be seen in Figure 4, where all surroundings are placed on a 160 mm by 100 mm PCB.

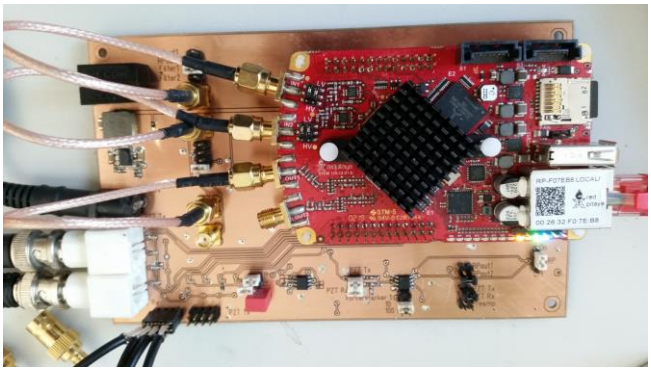

**Figure 4: Prototype of LILD electronics**

Since the ice detection principle is founded on the changing waveguide behaviour of the structure, these changes have to be measured. Therefore wave pulses are sent into the structure. To minimize higher harmonic distortions, one pulse consists of a number of periods of the basic carrier frequency overlaid with a Hann window. In preliminary experiments, a number of five to ten periods within the pulse have proven to be a good compromise between pulse duration and energy input into the structure. Too short pulses do not introduce enough energy for detection. If the pulse contains too many periods, it becomes too long to provide a sufficient separation of the different lamb wave modes with different travelling speeds. Detecting the pulses individually is critical for the sensor because an ice accretion acts differently on the modes.

To illustrate this, Figure 5 shows a sample measurement at a simple beam with a travelling distance of 30 cm. The transmitted pulse is shown in blue (ASend), whereas the received signal is plotted in red (ARec). It can be seen first, that the received signal also shows a pulse parallel to the sent pulse. This is intentional since the sent pulse is modulated onto the received signal. It allows a precise measurement of the lag time between the sent pulse and the received pulses if the sent pulse is added to the receiver signal. Second the received signals shows several pulses, which are a superposition of different lamb wave modes and signal reflections at the ends of the beam.

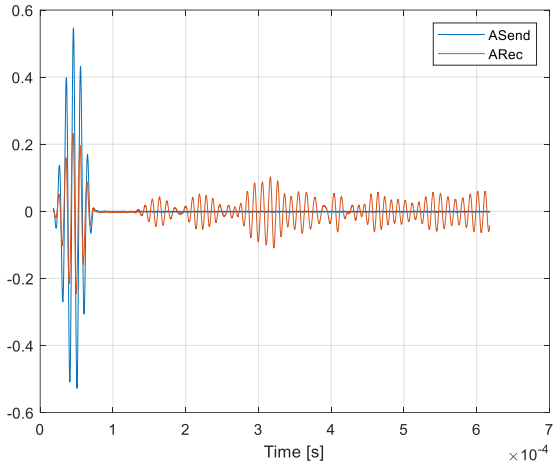


**Figure 5: Transmitted pulse (ASend, blue) and received pulses (ARec, red) of a sample measurement**

The main challenge in this primary signal analysis is to precisely determine the amplitude of all received pulses and their lag time with respect to the sent pulse. Therefore the maximum of the envelope function of the pulse has to be found. Since only a few periods are present within the Hann window, one cannot simply look for the maximum, why the data are filtered first to obtain the amplitude of the envelope function. This amplitude function is numerically differentiated afterwards to identify the negative slope zeros of the differentiation. They indicate a maximum in the amplitude.

Figure 6 shows the corresponding curves to the described method. The received data are shown in blue with the transmitted pulse in the beginning and all received pulses from 100µs onward. In red (Amp) the received signal is filtered to remove the carrier frequency of the lamb wave so that only the envelope curve of the pulses remains. The differentiation of the envelope curve is shown in orange (DAmp). As last, the negative slope zeros of the differentiated curve are shown as purple circles, where the maximum values of the envelope curve can be found (Max).

In the end, a table of lag time an amplitude for all identified pulses is provided, which allows to detect changes in the amplitude as well as changes in the lag time between the first pulse, which is the transmitted one, and all subsequent received pulses.

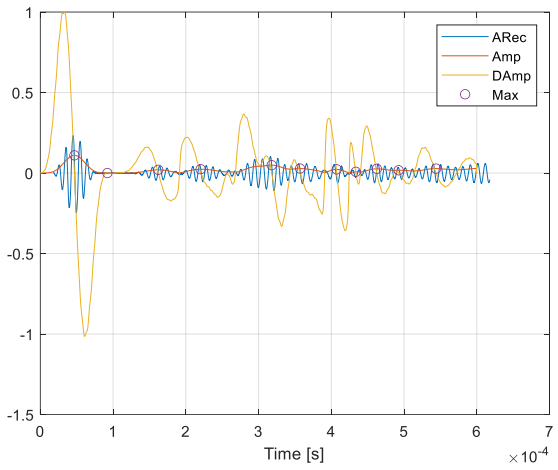


**Figure 6: Amplitude and lag time detection of sample measurement**

The second part of the signal analysis is to detect the presence of ice by the changes of pulse amplitude and lag time. Since the structural parameters of different types of ice are varying widely with temperature and the type of ice, simulations will not help to identify the impact of icing onto the wave guide behaviour. Therefore experiments in icing wind tunnels, where test airfoils can be exposed to artificial icing conditions, will be undertaken.

## IV. Wind Tunnel Demonstrator

For the wind tunnel experiments a test airfoil section is needed. With respect to the planned flight tests in the project, this airfoil section is supposed to be comparable to the location of the flight test, which will take place on a wing pylon structure used to mount special containers for atmospheric measurements below the wings. The leading edge of this pylon is perfectly suited for the LILD sensor since it is prone to icing and does not have ribs or spars which can create an excessive amount of interferences rendering the lamb wave measurement impossible.

For the wind tunnel tests, the leading edge airfoil is therefore set as a basis for the test section. The rear part has been shortened to reduce the size of the section and to make it fit the wind tunnels. Finally, a 50 cm span, 120 mm thick and 495 mm chord airfoil section has been designed for wind tunnel testing. It contains three sensing channels where wave pulses are sent along the span of the airfoil: One at the leading edge front, a second at the leading edge in front of the main spar and a third one behind the main spar. The position of the three channels is shown in Figure 7.

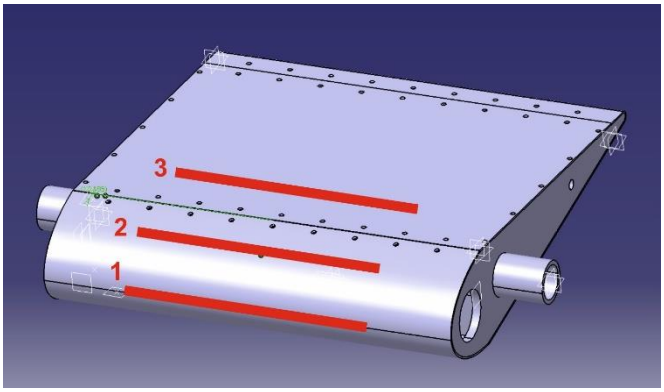


**Figure 7: Wind tunnel test airfoil section with three wave pulse channels**

As written before, piezoelectric transducers have been used for transmitting and receiving the wave pulses. To increase the signal amplitude, two patches have been used in parallel as transmitter. A photo of the transducers attached to the inside of the leading edge part is provided in Figure 8 with a one Euro coin for size reference.

**Figure 8: Transmitter piezoelectric patches compared to Euro coin**

This demonstrator has been mounted in two wind tunnels at the Technical University of Braunschweig: For first tests, a small wind tunnel at the Institute of Mechanics and Adaptronics (IMA) has been used. Finally icing wind tunnel tests took place within the SENS4ICE campaign at the Institute of Fluid Mechanics (ISM).

This wind tunnel has been upgraded and calibrated before and within the SENS4ICE project to produce a bi-modal SLD cloud in the Freezing Drizzle envelope specified in Appendix O. More information about the design of the wind tunnel is provided in [6]. A photo of the test setup in the ISM wind tunnel is shown in Figure 9.

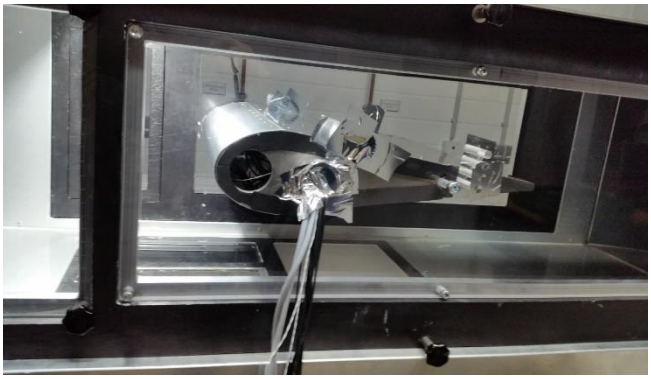

**Figure 9: Test airfoil installation in ISM wind tunnel**

## V. Signal Analysis and Wind Tunnel Results

### A. *Preliminary tests with intermittent icing*

To identify the effect of ice accretion on the received pulses, measurements have been performed in IMA wind tunnel. There the spraybar has been activated for 30s to accumulate ice in the structure. After this, the measurement was performed and another 30s of ice accretion was started. In total, several measurements have been undertaken with different air temperatures and summed icing times of up to five minutes. After all icing cycles, the thickness of the ice layer was measured on the leading edge using a preheated ruler, which was melted through the ice to touch the airfoil leading edge.

As result of these measurements, some clear trends can be stated:

- The first received pulse shows the greatest influence
- Small ice thicknesses below 1 mm lead to a distinct reduction of the received amplitude and an increase of the pulse lag time
- The loss of amplitude and increase of lag time is visible for all temperatures

To give an impression, Figure 10 shows the amplitude of the first received pulse over the lag time for a measurement frequency of 300 kHz and an icing time of 5 min, which corresponds to a 2.5 mm thick layer of ice. It can be seen that the amplitude is reduced already at ice thicknesses below 1 mm. This amplitude reduction finally saturates with a thickness of more than 2 mm, instead the lag time is increased.

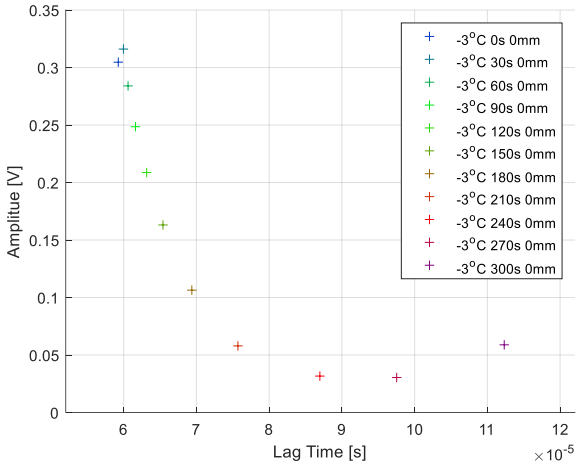


**Figure 10: Sample measurement made in IMA wind tunnel with -3°C ambient temperature with 300 kHz measurement frequency**

### B. *Icing wind tunnel tests with continuous icing*

In the second wind tunnel campaign at ISM, the measurement pattern was chosen to a more realistic manner: The spraybar was switched on for a certain time and the wave transmission behaviour was measured with 1Hz during the measurement time. At the end of the measurement, the ice thickness was measured the same way with a heated ruler. Within these tests, clear ice and mixed ice have been observed on the leading edge of the airfoil.

**Effect of icing on received pulse amplitude**

In contrast to the initial measurements, the amplitude reduction of the received pulse was not consistently obtainable. In some conditions, the amplitude shows a short increase and a decrease afterwards, which is already slightly visible in the IMA data Figure 10 too. In a variety of measurements, the amplitude increases for a much longer time or even shows oscillations. Three exemplary measurements for a frequency of 300 kHz are shown in Figure 11, where the amplitude change is plotted over the measurement time beginning with a clean airfoil without ice accretion. Additionally the active time of the spray bar is overlaid to identify start and end of ice accretion.

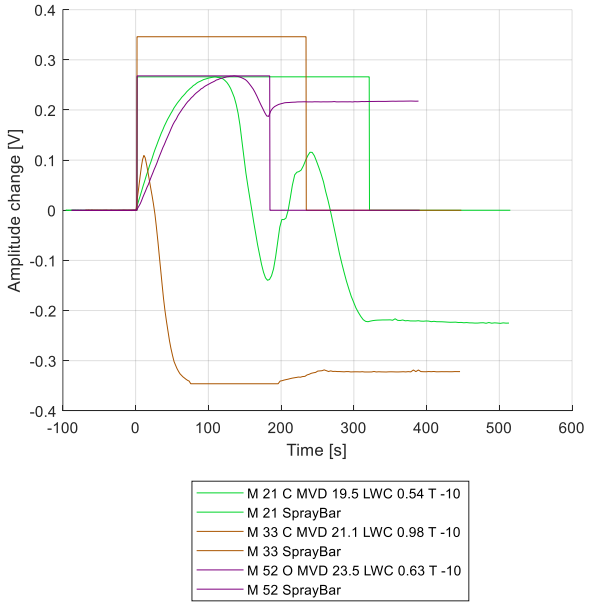


**Figure 11: Amplitude change for three exemplary measurements in ISM wind tunnel with 300 kHz measurement frequency**

While measurement 33 shows a short amplitude increase followed by a steep decrease, the other two measurements produce an increasing amplitude, which decreases much later. Therefore the amplitude change is a very sensitive indicator for a beginning ice accretion on a clean structure, but it is not well suited to determine the ice thickness or the end of the ice accretion alone.

The supposed reason for these different results to the initial measurements consists in the presence of much higher temperatures compared to the initial measurements shown in Figure 10. There the spraybar was activated for 30 s and the ice layer was allowed to cool down to the ambient temperature before the measurement was started. In contrast, the data shown in Figure 11 were obtained during ice accretion, where latent heat from freezing increased the temperature as shown in Figure 12**.** There the temperature measured at the location of the transmitter patch at the inside of the airfoil is shown.

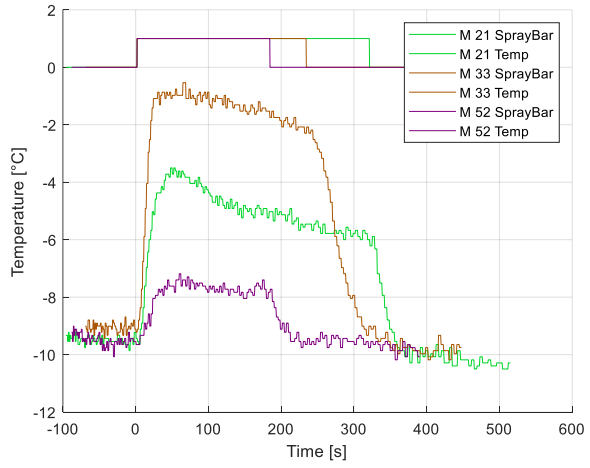


**Figure 12: Structural Temperature at transmitter**

It is clearly visible, that the temperature first rises with the beginning of ice accretion. Second the temperature increases differs with the icing conditions. Comparable temperature patterns have also been measured by González [7].

Due to the remarkable change in the temperature within the ice accretion process, it is assumed, that the damping characteristics of the ice layer on the structure and by this the amplitude change is of a strong dependence from temperature. Furthermore the ice accretion is expected to be higher when the droplets are hitting the cold airfoil before it is warmed up by latent heat release. For these reasons there is no easy relationship between the received amplitude and the ice thickness, since the ice shape and type as well as the temperature distribution need to be known.

**Effect of icing on received pulse lag time**

As shown in Figure 10, an ice accretion increases the lag time between the sent pulse and the received pulse. Therefore the lag time may be a better indicator for the identification of the ice thickness and the end of ice accretion. To prove this expectation, Figure 13 shows the change in lag time for the same three measurements, which have been displayed in Figure 12. At a measurement frequency of 150 kHz the lag time shows the most sensitivity to ice accretion.

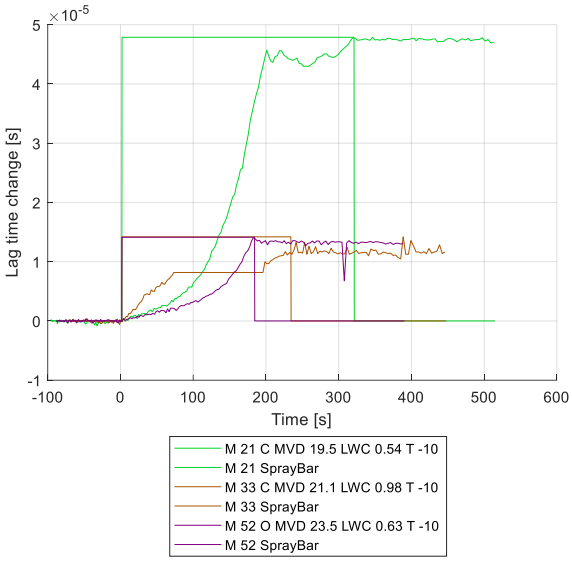


**Figure 13: Lag time change for three exemplary measurements at 150 kHz measurement frequency**

There it can be seen, that the lag time increases for all three measurements. Furthermore the increase stops, when the ice accretion ends, therefore the lag time is a good indicator for the end of the ice accretion period. The beginning of the accretion is not as clearly indicated, since the signal is noisy and therefore false alarms are to be expected.

In addition, correlations have been made on the available data between the ice thickness and the lag time change. This does not provide a definitive relation, but the ice thickness could be calculated based on the lag time increase with an error below 30% for most of the measurements.

One issue still is visible: When looking at measurement 33 in Figure 13, it can be seen that the lag time change ends before the end of the ice accretion period. The reason for this effect arises from a loss of signal since the received

amplitude is too small to extract the pulse signal. This has to be taken into account when analysing the sensor data.

**Wind tunnel test conclusions**

Finally 38 different icing condition cases have been measured in the ISM wind tunnel experiments, which spread into 12 bi-modal App O freezing drizzle and 26 App C cases. The IWT test points and test procedure have been carefully chosen to study the repeatability, fault tolerance and endurance aspects. The minimum response time of the sensor (critical for the certification) was computed for each the of test point cloud conditions conforming to the MOPS specified ED103-A. The minimum response time enables an unbiased and consistent comparison of different sensors tested at different IWT in the SENS4Ice project.

The main goal of the experiments was to detect the beginning of icing conditions and ice accretion with a preferably short response time. Figure 14 shows the measured response time vs. the required response time depending on the icing conditions, which has been defined within the project divided into App C and App O. It can be seen, that the LILD sensor is able to detect all cases with a relatively short response time in the range of a few seconds. For that reason the measurement campaign was successful.

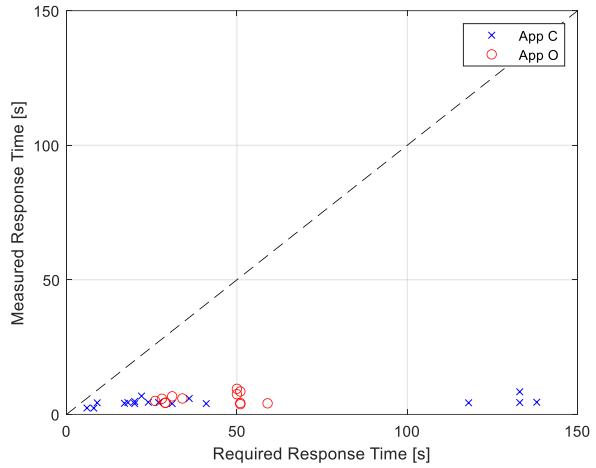


**Figure 14: Measured response time vs. required response time**

## VI. Conclusion and Outlook

The aim of the SENS4ICE project is to develop and test a variety of icing sensors for the use at aircraft. Withinthese activities, the LILD sensor has been investigated which is based on a changing behaviour in the transmission of ultrasonic lamb waves through a structure, which is prone to ice accretion. Since a flight test is planned within the project, the main activities were focused on the design of a flight test ready hardware, which is able to provide the signal generation and signal acquisition as well as all filters and the final signal analysis. This resulted in a prototype hardware, which is of small size and only draws less than 10 W of power, so that even a simple cellphone supply will be sufficient.

In a second step, a filter algorithm has been set up to find all received pulses, which then allows to determine the amplitude of the received pulse as well as its lag time after the transmitted pulse. Changes in lag time and amplitude have been identified to be influenced by the presence of ice.

To further quantify the influences, wind tunnel tests have been undertaken with the result, that the presence of ice is indicated with a very small response time by a change of the received pulse amplitude. In parallel, the lag time increases with the ice thickness, which can be used to obtain the ice thickness as well as the end of the ice accretion.

In the short term future, the flight test needs to be prepared. Therefore a new sensor hardware is under development containing an interface to communicate with the aircraft systems. A CAD model for a single sensor electronics box can be seen in Figure 15.

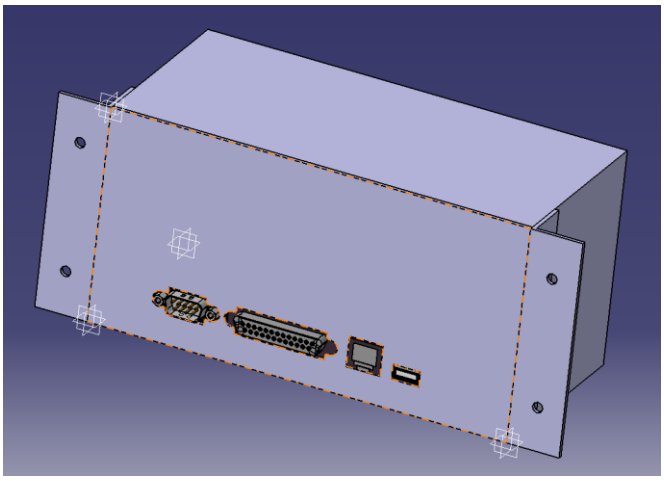

**Figure 15: CAD model of LILD sensor electronics box**

In parallel, the signal analysis software needs to be updated for the ice accretion detection based on the amplitude change and the increase of lag time.

In long term, the LILD sensor needs more test data to further investigate the correlation between different types of ice, different temperatures and icing conditions and the lag time and amplitude change for multiple frequencies. This may lead to a further discrimination of the icing conditions as well as a more precise detection of icing and ice thickness.

## Acknowledgment

This project has received funding from European Union's Horizon 2020 research and innovation program under grant agreement number 824253.

## VII. REFERENCES


[1] G. A. Hoover, „Aircraft ice detectors and related technologies for onground and inflight applications,“ GALAXY SCIENTIFIC CORP MAYS LANDING NJ, 1993.

[2] Collins Aerospace, „Primary & advisory ice detection systems,“ [Online]. Available: https://www.collinsaerospace.com/-/media/project/collinsaerospace/collinsaerospace-website/product-assets/marketing/i/ice-detection/primary-and-advisory-ice-detection-systems.pdf?rev=7f0a0cacd46147b8a5a21683ba200b3c.

[3] Collins Aerospace, „Optical Ice Detector (OID),“ 2022. [Online]. Available: https://www.collinsaerospace.com/-/media/project/collinsaerospace/collinsaerospace-website/product-assets/marketing/o/optical-ice-detector-data-sheet.pdf?rev=a2d78e0e0fe940159ac4ccc37a9e8089&hash=4CCD1CF28939EF9665B08C42EA81B3AD.

[4] PI Ceramic, „P-876 DuraAct Patch Transducer,“ 2022. [Online]. Available: https://www.piceramic.de/de/produkte/piezokeramische-aktoren/flaechenwandler/p-876-duraact-flaechenwandler-101790/.

[5] Red Pitaya, „STEMlab 125-14,“ 2022. [Online]. Available: https://redpitaya.com/stemlab-125-14/.

[6] S. E. e. a. Bansmer, „Design, construction and commissioning of the Braunschweig Icing Wind Tunnel,“ *Atmospheric Measurement Techniques*, pp. 3221-3249, 2018.

[7] M. e. a. González del Val, „Icing Condition Predictions Using FBGS,“ *Sensors*, Bd. 21, p. 6053, 2021.